2D ICED AIRFOILS AERODYNAMIC PERFORMANCE MEASUREMENTS AND SIMULATIONS

J. Decours, A. Le Pape

Applied Aerodynamics Department, ONERA
BP72, 92322 Châtillon Cedex, France
e-mail: julien.decours@onera.fr
arnaud.lepape@onera.fr

Key words: Aerodynamic, Performance, Icing, Measurement, Simulation, Structured

Abstract: *The prevision of aerodynamic performance in icing conditions is a critical security topic for helicopters manufacturers. Therefore, two clean airfoils and three ice shapes have been tested in the ONERA S3MA wind tunnel to establish a large aerodynamic performance data base. Those data have been used to validate the numerical simulations to finally allow iced airfoil polar tables for comprehensive codes generation. As a result, 2D Reynolds average Naviers-Stokes computations have been performed on those clean and iced airfoils. The ONERA object oriented structured code, elsA was used together with the DLR unstructured code, TAU to forecast the important performance penalties due to the different ice shapes.*

1 INTRODUCTION

The prevision of aerodynamic performance in icing conditions is a critical security topic for helicopters manufacturers because ice reduces lift and causes stall to occur at much lower blades angles of attack. Also, even if the lift is still large enough to sustain the helicopter flight, the drag increase due to the ice shape implies an important power rise detrimental in term of rotorcraft performance. Thus, it is important to understand how the different ice shapes can affect the blade aerodynamic performance [1] [2]. As a result, ice shapes have been divided in four main categories to describe the different flow physics and aerodynamic effect [3]. The four categories were: roughness, streamwise ice, spanwise-ridge ice, and horn ice. The horn ice flowfields, which are helicopter blades specific cases, are characterized by large flow separation. The separation location is known to be relatively fixed by the geometry of the ice shape, but the aerodynamic performance penalties due to ice are very difficult to estimate. Therefore, different methods have been used to forecast the iced airfoils performance [4] [5]. And finally, wind tunnel tests and numerical simulations have been realized in order to improve tools ability to estimate the aerodynamic performance penalties due to ice [6].

In the present study, tests in the ONERA S3MA 2D wind tunnel were performed to measure the aerodynamic performance of clean and iced helicopter airfoils. Two clean airfoils and three ice shapes with a rising complexity were investigated for a wide range of Mach numbers and angles of attack and two Reynolds numbers, matching the helicopter blades flight conditions. The three ice shapes were equipped with pressure taps to ensure a high-quality of the lift and pitching moment coefficients measurement and integration. The drag coefficient was precisely estimated with wake measurements.

The important database resulting from the wind tunnel tests is used to validate the numerical simulations to finally allow iced airfoil polar tables for comprehensive codes genera-

tion. Therefore, 2D Reynolds Average Naviers-Stokes computations have been performed on clean and iced airfoils. The ONERA object oriented structured code, *elsA* [7] was used together with the DLR unstructured code, TAU [8]. The most comparable numerical schemes for both codes have been used, with a k-ω turbulence model to solve a fully turbulent flow.

The experimental setting, measurement and results are further discussed in the first part of the paper. Then, details on numerical methods are given in the second part of the paper, in addition to detailed comparisons between structured and unstructured code predictions with the experimental data base. Finally, results are compared in order to draw global conclusions on the aerodynamic performance of helicopter iced airfoils.

2 AIRFOILS AERODYNAMICS PERFORMANCE MEASUREMENTS

2.1 Experimental settings

The tests were conducted in the ONERA S3MA wind tunnel, which is a blow-down pressurized transonic wind tunnel. The test section size is 0.56x0.78 meters and Mach number from 0.3 and up to 1.3 can be reached. The wind tunnel roof and floor are porous and side walls are equipped with portholes that ensure an optical access. It has to be mentioned that numerous tests were performed in this wind tunnel in the 80's and 90's on the OA209 and OA213 clean airfoils.

The OA213 and OA209 models are presented in Figure 1. The clean airfoils models are made in steel and have a chord equal to 210 mm. Each model is equipped with respectively 103 and 94 pressure taps (Figure 2).

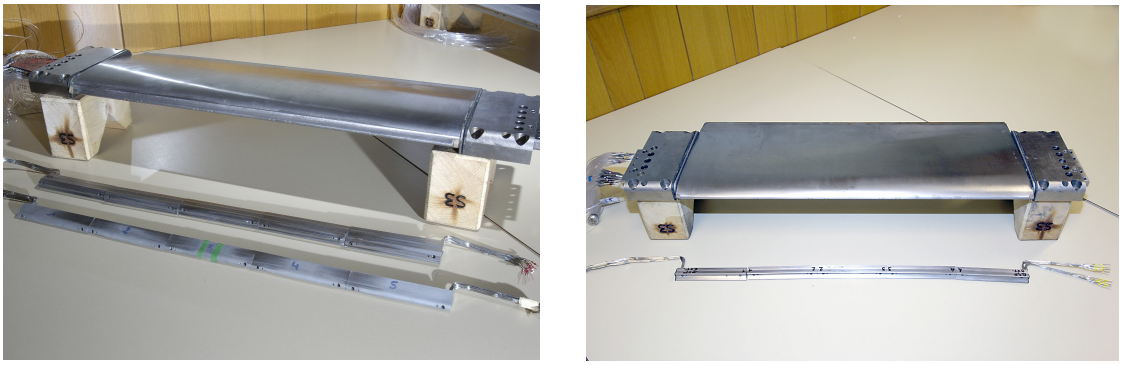

Figure 1 : Models of the OA213 and OA209 airfoils

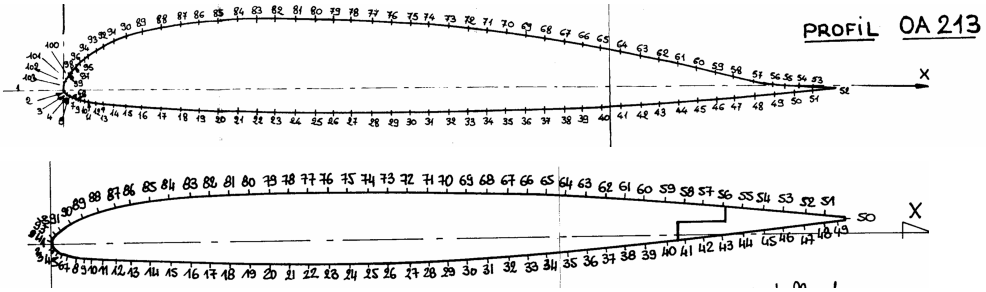

Figure 2 : Pressure taps distribution on OA213 (top) and OA209 (bottom) airfoils

Three iced leading-edges were built. The three ice shapes (Figure 3) correspond to typical ice accretions that can be found on helicopter rotor blades under icing conditions [9] [10]. The first ice shape correspond to an accretion at low speed (M=0.3), in the blade root area; this shape is tested with the OA213 airfoil. The second ice shape is typical of an accretion at medium air speed (M=0.45) at mid-span of the blade; this shape is tested with the OA213 airfoil. Finally, the third shape is typical of an accretion at Mach number around 0.7. Such iced shape can be found near helicopter blade tip; the Ice3 shape is tested with the OA209 airfoil. The three iced shapes have been milled by the model manufacture department of ONERA. Each shape is made of 5 pieces that are adapted and crewed on the leading-edge of the airfoil model. A particular attention is paid to the impermeability between each piece of the iced-leading edge and the model, which is ensured thanks to a very precise adaptation. The center piece of the iced shape is equipped with pressure taps distributed in 2 sections along the chord. A strong effort during the design process of these iced-trailing-edges has been devoted to the number of pressure taps: the aim was to optimize the pressure taps distribution in order to capture as accurately as possible the pressure gradients on the iced airfoil. Finally approximately 25 pressure taps (Figure 3) could be installed in the three iced shapes. This allows to have around 100 pressure taps distributed along the suction and pressure sides of each iced airfoil (the clean airfoil pressure taps are covered by the iced-leading edge). The final numbers of pressure taps available during the wind tunnel tests are summarized in Table 1.

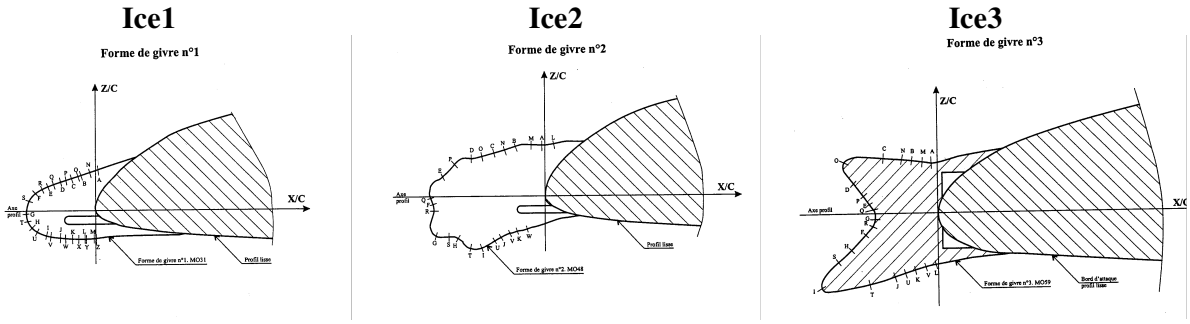

Figure 3: Iced-leading edges used for wind tunnel tests

Clean OA213	103 taps
BA shape 1	26 taps
BA shape 2	23 taps
OA213 + shape 1	98 taps
OA213 + shape 2	99 taps
Clean OA209	94 taps
BA shape 3	22 taps
OA209 + shape 3	101 taps

Table 1: Pressure taps distributed along the airfoil chord for each configuration

2.2 Test matrix

The test matrix was chosen to cover a wide range of the helicopter flight envelope, since one objective is to determine iced-airfoil polars to be used in comprehensive codes. The polars are measured at constant Reynolds over Mach number (ratio Re/M); tests were performed at 2 Re/M parameters in order to investigate the Reynolds number effect: Re1=8.10^6.Mach and Re2=4.10^6.Mach. For each clean or iced airfoil, around 8 polars (α from -3° to an angle of attack higher than $\alpha(Cz_{max})$) at Re1 and 4 polars at Re2 were measured. Finally a total of more than 60 polars from M=0.3 to M=0.95 were obtained, which represents more than 100 wind tunnel runs.

2.3 Measurements

The lift and pitching moment aerodynamic coefficients are determined by pressure integration thanks to the high number of pressure taps implanted in the models and in the iced leading-edges (Figure 3). The integration is made using a trapeze method with a parabolic correction at the leading-edge and the trailing-edge. Pressure measurements on the wind tunnel walls are performed in order to apply specific wall corrections designed for 2D tests.

The drag is measured thanks to wake measurements performed with 5 total pressure sensors and 4 static pressure sensors. These sensors are mounted on a motorized mast so that a sweep inside the wake could be performed during each test point. The repeatability of the aerodynamic coefficient measurements is very good and illustrated in Figure 4 for the shape3.

Strioscopy visualizations were also performed at each test points in order to investigate the flowfield topology, an exemple of visualization is presented in Figure 5.

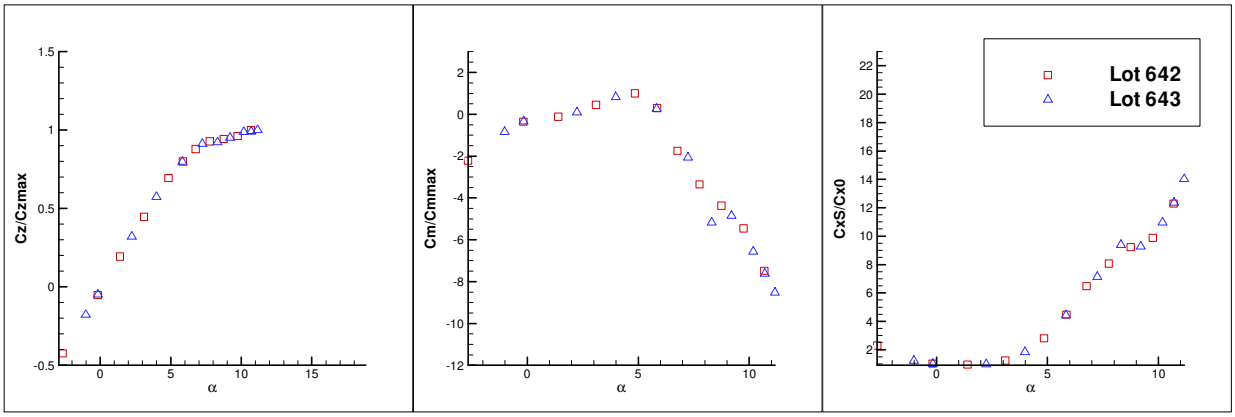

Figure 4: Repeatability on Cz, Cm and CxS coefficients obtained with the shape3

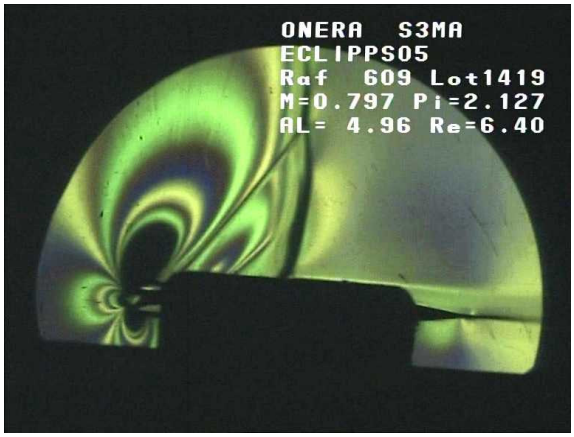

Figure 5: Strioscopic visualization of the flowfield topology around the ice shape3 at Mach 0.8 and 5° of angle of attack

2.4 Results

An example of the results obtained during the wind tunnel tests is plotted in Figure 6, where the lift and pitching moment coefficients measured on the clean and iced OA213 airfoils are plotted. One can notice the important lift penalty due to the ice, which is equivalent with both shapes 1 and 2. The iced leading-edges have also an important effect on the pitching moment coefficient which is highly perturbed. The pressure coefficient distributions along the chord used to obtain these aerodynamic coefficients are presented in Figure 7. One can notice the very good description of the pressure measurements on the iced airfoils.

The wind tunnel results will be more deeply discussed when compared to the *elsA* and TAU computations in the following paragraphs.

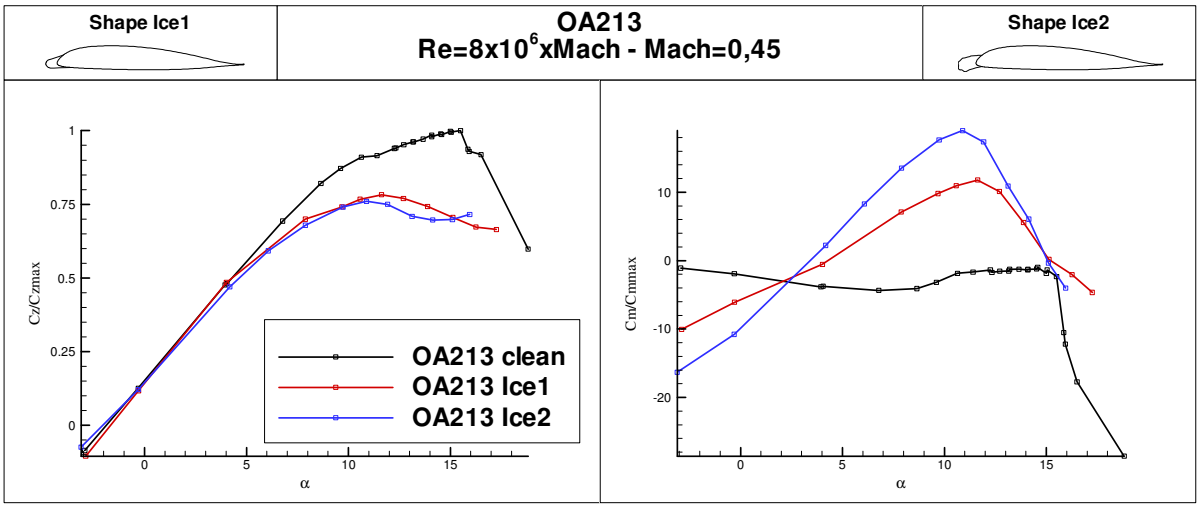

Figure 6: Lift and pitching moment coefficients measured on the iced and clean OA213 airfoil at Mach =0.45 and Re1

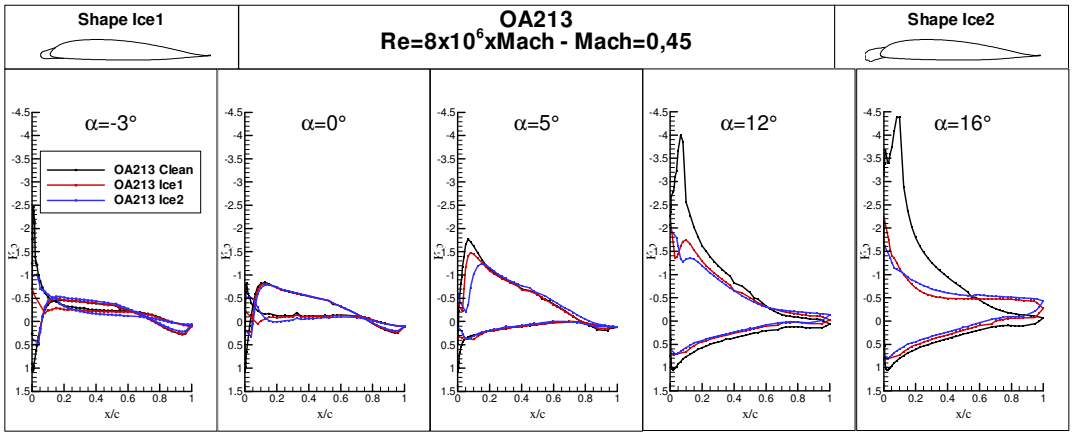

Figure 7: Pressure coefficients measured on the clean and iced OA13 airfoils at M=0.45 and Re1

3 AIRFOILS AERODYNAMIC PERFORMANCE SIMULATIONS

The simulations presented here are related to the configurations previously tested. Computations of clean and iced airfoils performance were carried out before the tests to have a good idea of the angle of attack range as well as the position of the pressure sensors making it possible to correctly discretize the pressure field on the airfoil.

3.1 Structured grid and numerical method

For the estimation of clean and iced airfoils performance, structured computations are performed with the code *elsA*. This multi-application object oriented solver, using the C++ and FORTRAN languages, is described in [7]. It is based on structured multibloc grids where the Navier-Stokes equations (RANS) are solved in a finite volume formulation.

A robust method of meshing using a classical 'C-H' grid topology with a single block around the profile was chosen and carried out with ICEM-CFD. The grids are rather fine and contain about 500 points on the airfoil, 140 in the normal direction and 50 in the wake. Concerning the iced airfoils cases, the grids contain roughly 350 points on the smooth part of the airfoil and between 160 to 210 points on the ice shapes. The grid around the iced airfoil and the detail of the three ice shapes are presented in Figures 8 to 11.

With regard to the numerical parameters, a second order in space discretization was used with a Jameson scheme including a scalar artificial viscosity with the Martinelli's correction combine with a LUssor implicit phase and a backward Euler time integration. Simulations are initialized with 20 laminar iterations. Then a fully turbulent field is calculated with a two levels 'V cycle' multi-grid. A Wilcox k-ω with SST correction turbulence model was chosen and the laminar-turbulent transition was not modeled. Here are only presented correctly stabilized computations, corresponding to stationary airflows. When it was not possible to stabilize the flows or when oscillations appeared in the numerical solution, in particular for the ice shape 3 with incidences higher than 6° at Mach 0.5, a unsteady numerical scheme was used to converge the solution.

The good convergence of the structured computation is presented in Figure 11 with the residual histories, which lose approximately 6 orders and in Figure 12 with the lift coefficient histories which look very stable, for increasing angles of attack.

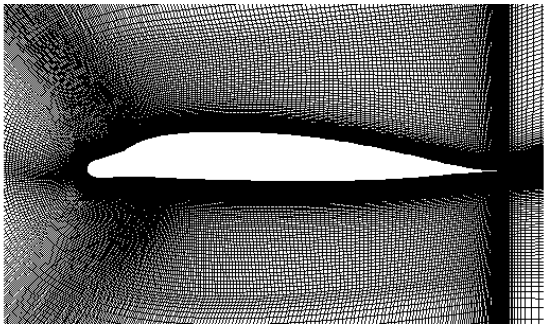

Figure 8: Structured grid around iced airfoil

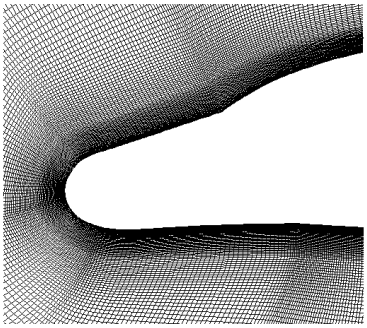

Figure 9: Structured grid around ice shape 1

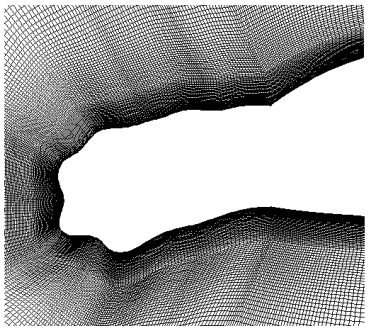

Figure 10: Structured grid around ice shape 2

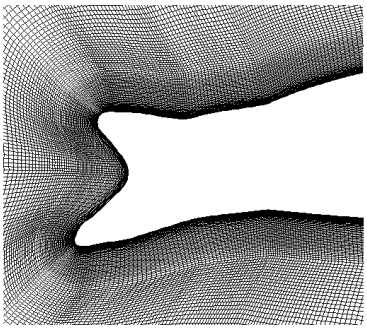

Figure 11: Structured grid around ice shape 3

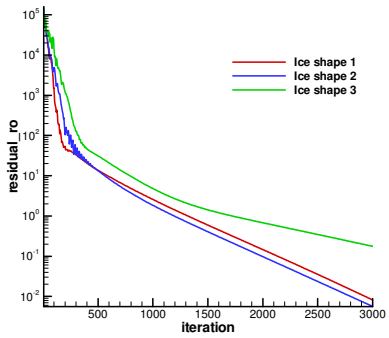

Figure 12: Residual histories of structured computations

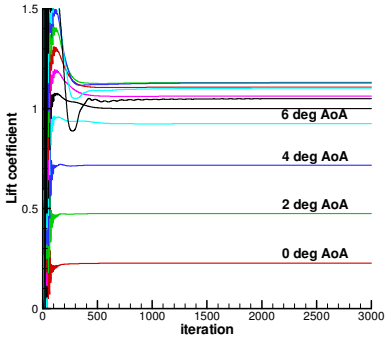

Figure 13: Lift coefficient histories of structured computations

3.2 Unstructured meshing and numerical method

In order to compare the clean and iced airfoils performance using an unstructured method, the TAU code from the DLR has been tested on the same shapes [8]. The grids were previously realized with the Centaur software, then the principal modules of the TAU code concerning pre-treatment, computation and adaptation were used to carry out unstructured simulations with its particular method.

The grid generation with the Centaur software is very ergonomic. A wild domain of 100 chords centered on the airfoil is defined with an average cell size in the chord direction, as well as a number of parallelepipedic sub-layers with a first cell size. A growing factor of the triangles cells is defined and the grid is automatically generated. Figure 14 presents the first grid obtained for the clean OA213: it contains approximately 700 points on the airfoil, for a total of 80000 elements including 20000 quadrangles.

Then the pretreatment phase allows imposing the numerical parameters, that is to say, a Jameson scheme coupled to fourth order Rung-Kutta time integration. A fully turbulent field is then calculated with a 'W cycle' four levels multi-grid. A Menter k-ω turbulence model with the compressibility correction of Wilcox was chosen to be as much comparable as possible to the structured computations with *elsA*. An adaptation on the pressure gradients is realized for each incidence after 2000 iterations on the first grid. This adaptation leads to a new grid which contains 30% additional points and approximately 900 points on the airfoil. Figures 15 to 17 present the grids after adaptation with 10° of angle of attack on the OA213 and the three ice shapes.

The good convergence of the computations is presented in Figure 18 with the history of the residuals, which lose approximately 4 orders during the first phase of calculation and still 2 orders after the adaptation of the grid but only for the small angles of attack. On the other hand for the high angles of attack the convergence after adaptation is not so efficient (reduction of approximately half an order). We notice in Figure 19 representing the convergence of the lift coefficient, that the adaptation has a considerable influence on the calculated value of the loads. With the increase of the angle of attack, the adaptation modifies the average value of the lift coefficient as well as the amplitude of the oscillations. In addition, different solutions could be obtained depending on the iteration at which the adaptation was carried out and the aerodynamic field and gradients on which it occurs. Consequently, the computations leading to oscillating flows are not retained for present analysis.

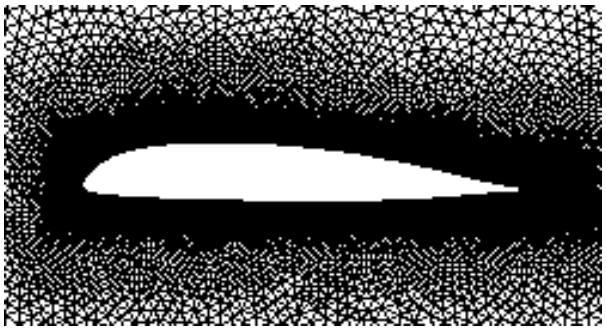

Figure 14: Initial unstructured grid around clean OA213

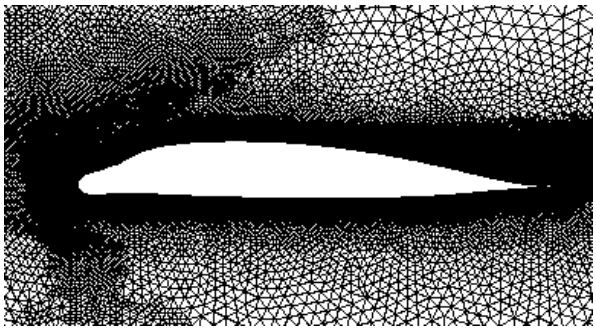

Figure 15: Unstructured grid around ice shape 1

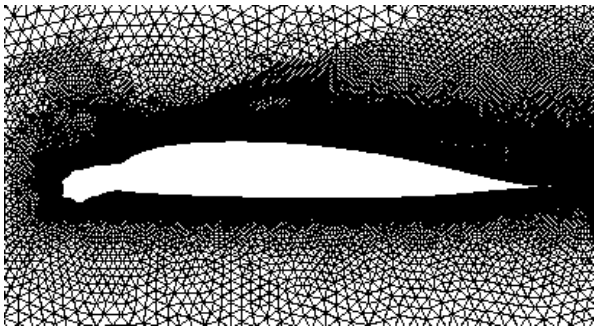

Figure 16: Unstructured grid around ice shape 2

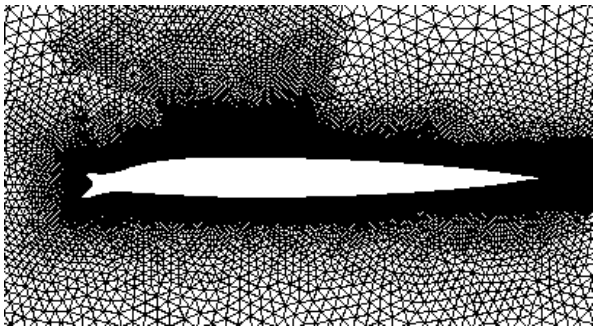

Figure 17: Unstructured grid around ice shape 3

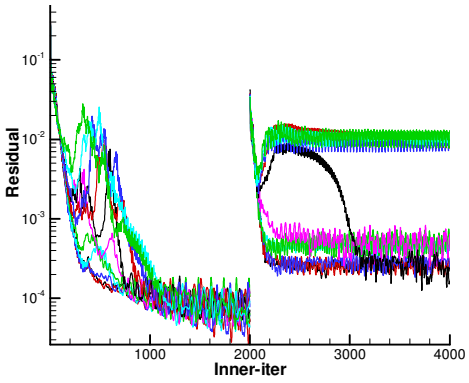

Figure 18: Residuals histories of unstructured computations with adaptation

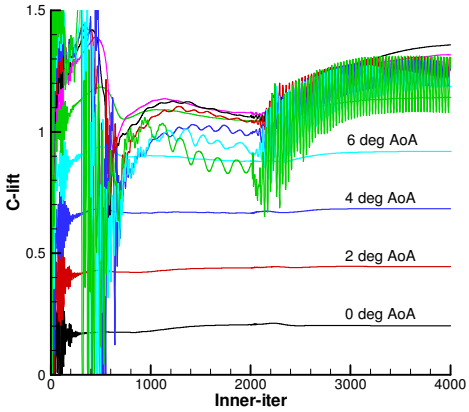

Figure 19: Lift coefficient histories of unstructured computations with adaptation

4 RESULTS AND DISCUSSIONS

The aerodynamic lift, drag and pitching moment coefficients calculated by the codes *elsA* and TAU and measured in S3MA on the clean OA213 airfoil and equipped with the two ice shapes at Mach 0.3 are presented in Figures 20 to 28. First of all, the ice shapes influence on the overall aerodynamic performance is well restored despite local deviations describe below.

In a more detailed analysis on the clean airfoil lift coefficient, we observe that the unstructured method does not capture any stall while the structured one suggests a smooth stall with a correct estimation of the maximum lift (Figure 20). Concerning the first ice shape, both codes predict a premature stall angle, but the unstructured one estimates a correct maximum lift level (Figure 21). Regarding the second ice shape, both code predictions are very similar in terms of lift coefficient, with an underestimation of the maximum lift angle of attack and level (Figure 22). Finally, for both codes, clean and iced airfoils, the linear part of the lift coefficient polar is well predicted. That is to say that the ice shape is well taken into account in both simulations in the useful range of angle of attack for helicopter blades. Since differences occur near stall, the estimation of maximum lift level, corresponding angle of attack and slopes is not so bad, despite a decreasing accuracy with the complexity of the form.

Concerning the drag coefficient, it has to be noticed that the TAU code gives a good estimation for the clean airfoil but also for the two ice shapes, in spite of the fully turbulent as-

pect of calculations (Figures 23 to 25). On the contrary, the drag is overestimated for the clean airfoil as well as for the two ice shapes by the structured code. Taking into account the laminar-turbulent transition would certainly make it possible to limit this overestimation or delay of the stall angle of attack. Nevertheless, the trends due to the ice shapes are correctly captured in terms of drag levels. One will keep in mind the very significant number of points on the airfoil for TAU code simulations after adaptation. Also, a very detailed attention will be paid thereafter to the estimated drag coefficients, since its integration on the blade leads directly to the torque increase necessary to maintain the rotation of the iced rotor.

In terms of pitching moment coefficients, the general levels and the slope reverse effect are very well reproduced by both simulations even if the angles of stall remain underestimated. That is to say the ice accretion and the chord increase due to the ice shapes are correctly taken into account. Regarding the clean airfoil, the *elsA* code simulates a behavior close to the tests although the mean level is approximately 30% shifted (Figure 26). On the other hand, the TAU code gives levels very comparable with the tests although the shape of the curve is less regular. Concerning the first ice shape, the *elsA* code correctly reproduces the experimental curve shape, but still with premature stall (Figure 27). This time, it is the TAU code which presents a shift level from approximately 30% but a correct stall angle, whereas it was underestimated in term of lift coefficient. With reference to the second ice shape, the *elsA* code gives a good pitching moment coefficient estimation, but still with premature stall (Figure 28). It is the same trend with the unstructured code but with a maximum moment overestimation. Finally, the forecast of the important fluctuations and slope reversion, due to the chord increase with the ice shapes, on the pitching moment coefficient is rather good in spite of the small variations of stall angle.

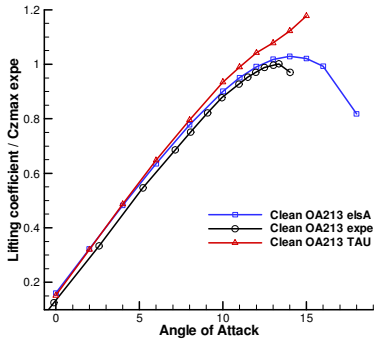

Figure 20: Lift coefficient for the clean OA213 at Mach 0.,3

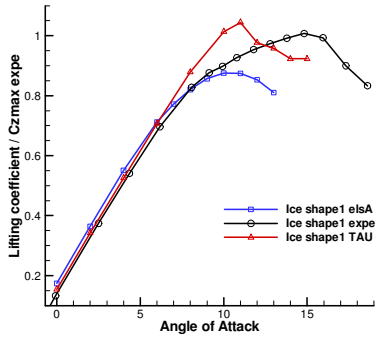

Figure 21: Lift coefficient for the ice shape 1 at Mach 0.3

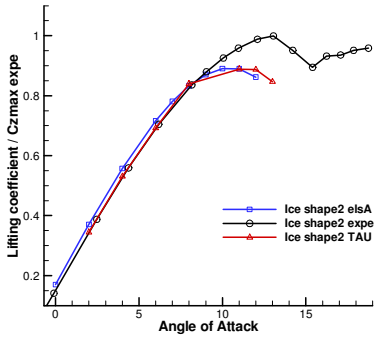

Figure 22: Lift coefficient for the ice shape 2 at Mach 0.3

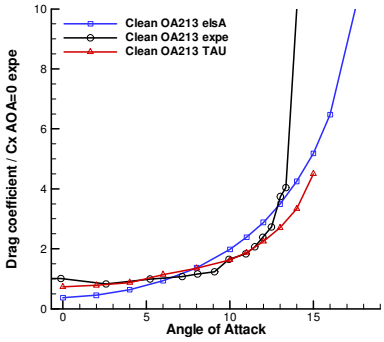

Figure 23: Drag coefficient for the clean OA213 at Mach 0.3

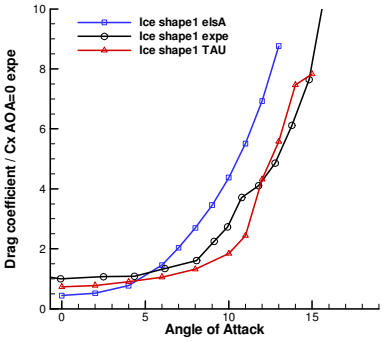

Figure 24: Drag coefficient for the ice shape 1 at Mach 0.3

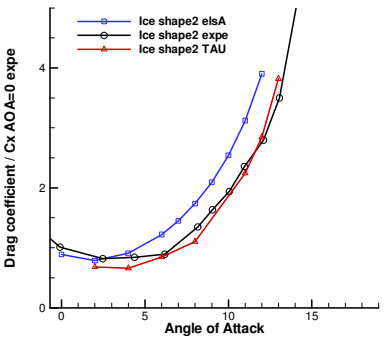

Figure 25: Drag coefficient for the ice shape 2 at Mach 0.3

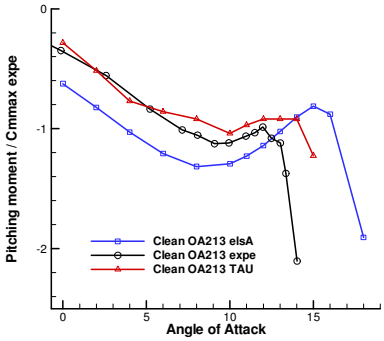

Figure 26: Pitching moment coefficient for the clean OA213 at Mach 0.3

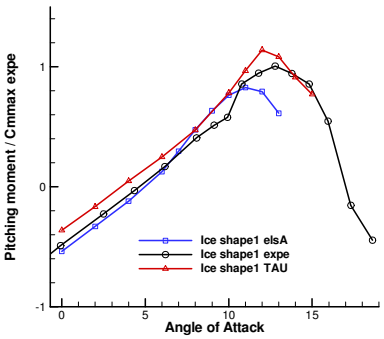

Figure 27: Pitching moment coefficient for the ice shape 1 at Mach 0.3

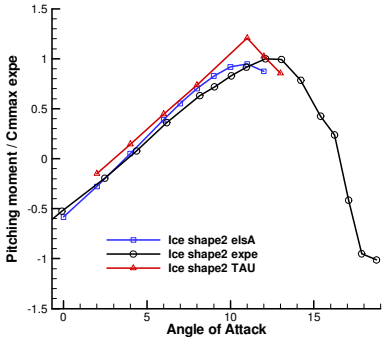

Figure 28: Pitching moment coefficient for the ice shape 2 at Mach 0.3

Numerical simulations have been performed on the clean and iced OA209 airfoils with the *elsA* code until 12° of angle of attack. It was not possible to obtain properly converged computations for the third ice shape at angles of attack higher than 4° with the unstructured TAU code.

The lift, drag and pitching moment coefficients calculated on the clean OA209 and equipped with the third ice shape at Mach 0.5 are presented in Figures 29 to 31. With regard to the lift coefficient, comparable results to those obtain on the OA213 airfoil are obtained. The stall appears prematurely with the third ice shape and the maximum lift is underestimated by approximately 15%. The double horn ice shape generates large separated flows around the leading edge producing important unsteady oscillations (Figure 32). Therefore, to ensure good quality results, unsteady computations were performed for high angles of attack. These simulations produce good predictions in terms of drag coefficient. Indeed, the third ice shape important drag increase effect is fairly well predicted compared to the other ice shapes. The Mach number increase could also be a reason in the improvement of the results quality. Concerning the pitching moment, the very high values reached with the third ice shape are underestimated. However, the code reproduces well the double change of sign due to the double horn shape.

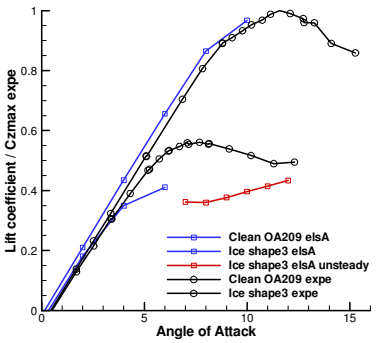

Figure 29: Lift coefficient for the clean and iced OA209 at Mach 0.5

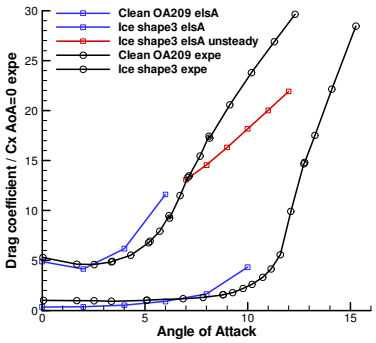

Figure 30: Drag coefficient for the clean and iced OA209 at Mach 0.5

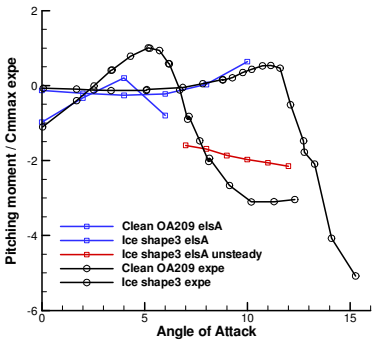

Figure 31: Pitching moment coefficient for the clean and iced OA209 at Mach 0.5

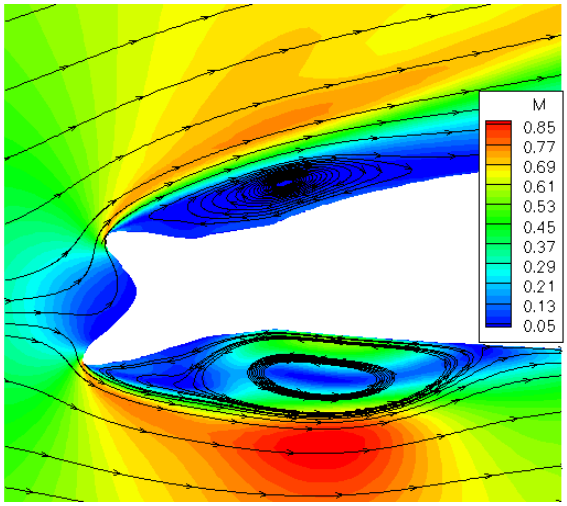

Figure 32: Mach number contours around iced OA209 at Mach 0.5 and 7° angle of attack

The pressure coefficients on the clean OA213 airfoil at Mach 0.3 and 10° of angle of attack calculated by both *elsA* and TAU codes and measured in S3MA are presented in Figure 33. A very good agreement between both codes is observed, but with a light over-estimation of the pressure coefficient compared to the experimental values. On the pressure side, both codes overpressure underestimation is equivalent, as well as the overspeed small peaks of the suction side. The main difference occurs on the suction side of the trailing edge: the pressure plateau indicating the separation of the flow is larger with the structured code. This numerical agreement confirms the previous results, that is to say the numerical approach is not siof primary importance in the linear part of the polar.

With reference to the first ice shape, the pressure coefficients at Mach 0.3 and 10° of angle of attack are presented in Figure 34. Notable differences between the two codes are now observable. The *elsA* code prediction of the maximum lift is slightly lower than the tests whereas the TAU code still before stall, over-estimates it (Figure 21). Indeed, the *elsA* code stalls a few degrees earlier than TAU calculations. This is in agreement with the pressure distribution in Figure 21. On this first smooth ice shape, the laminar-turbulent transition calculation could have a favorable effect on the prediction of performance of the *elsA* code.

At last, the pressure coefficients on the ice shape 2 at Mach 0.3 and 8° of angle of attack are presented in Figure 35. The good results on the integrated loads of the codes are confirmed by the pressure coefficients. Although the code *elsA* under evaluates the depression on the suction side slightly, the shape of the curve remains correct on the suction side. The code TAU presents a distribution of pressure very close to the experimental ones considering the complexity of the shape.

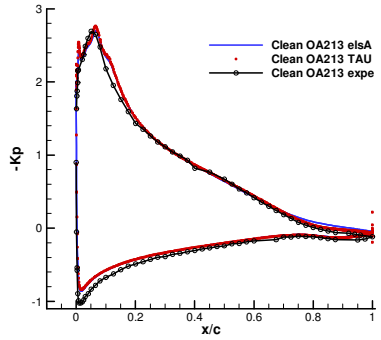

Figure 33: Pressure coefficient distribution on the clean and iced OA213 at Mach 0,3 and 10° angle of attack

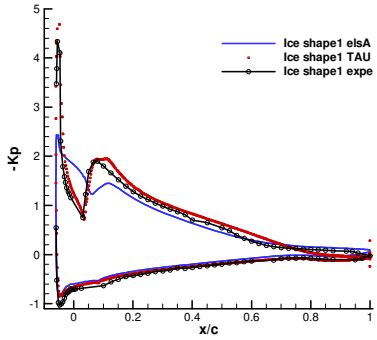

Figure 34: Pressure coefficient distribution on the ice shape1 at Mach 0,3 and 10° angle of attack

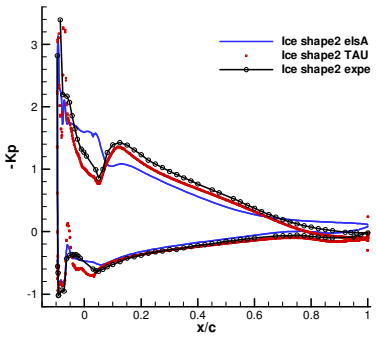

Figure 35: Pressure coefficient distribution on the ice shape2 at Mach 0,3 and 8° angle of attack

To sum up, the structured code allows predicting good trends, even for complex flows such as around ice shape 3, but has a delay in terms of stall angle of attack on the clean airfoil and a lead with the two ice shapes. The turbulence modeling, including the transition on those complex ice shapes could be a reason for this remaining gap on the angle of attack. On the other hand, the unstructured code returns good levels estimations, especially in terms of drag coefficient, but polar curves seams less stable. The important number of points on the airfoil and the adaptation process for each angle of attack can be an explanation for the good results obtained with the unstructured method (better accuracy in the pressure integration).

5 CONCLUSIONS

Wind tunnel tests of clean and iced airfoil aerodynamic performance carried out in S3MA wind tunnel have been presented. Many polars on OA213 and OA209 clean airfoils and equipped with complex ice shapes were acquired for a large range of Mach number representative of the real helicopter flying conditions.

The penalties due to the ice shapes have been established very important. Depending on the cases, the lift coefficient levels could be reduced by a factor of 2 and drag coefficient levels multiplied by a factor of 20. Moreover, the ice shapes lead to strong variations of the pitching moment coefficient likely to produce important mechanical constraints on the rotor head as well as controllability issues.

Then, 2D Reynolds Average Naviers-Stokes computations have been performed on clean and iced airfoils. The ONERA object oriented structured code *elsA* was used together with the DLR unstructured code TAU. From the numerical point of view, the important penalty due to the ice shapes on the airfoils aerodynamic performance is well restored by the simulations, in spite of local deviations. Concerning the lift coefficient, the deviations are small in the linear part of the polar. On the other hand, both codes still miss accuracy in the maximum lift area and tend to anticipate stall. In term of pitching moment, the results are very promising considering that strong variations due to the prominence of the ice shape are well reproduced, with correct levels. For the drag coefficient, the unstructured TAU code gives good results on the clean and iced airfoils, whereas efforts still remain to be made with the structured *elsA* code which tends to over-estimate the drag. Taking into account the laminar-turbulent transition would make it possible to improve the essential drag estimation, since it leads to the torque needed to maintain the constant rotor speed.

Studies on ice accretion and performance degradation will continue at ONERA considering 3D aspect occurring on helicopter rotor.

ACKNOWLEDGMENT

The authors would like to gratefully thank all the wind tunnel people involved in these tests and in particular Evelyne Simon who has highly contributed to the success of this wind tunnel campaign. A grateful thank is also presented to the DPAC for its financial support and the DLR for using the DLR TAU code at ONERA.

6 REFERENCES

[1] X. Chi et Al. "2-D and 3-D CFD simulations of clean and iced wings", 44th Aerospace Sciences Meeting and Exhibit, January 9-12 2006, Reno, Nevada.

[2] Final report of GARTEUR AG-32: "Prediction of performance degradation due to icing for 2D configurations", GARTEUR TP 143, 2003

[3] M.B. Bragg, A.P. Broeren, L.A. Blumenthal, "Iced-airfoil aerodynamics", Progress in aerospace sciences 41 (2005) 323-362

[4] R. Hindman, N. Crist, B. Williams, X. Chi, Y. Choo, and T.I-P. Shih, "Q3D-wing: Validation of a modern lifting-line method for application to clean and iced wings", 44th AIAA Aerospace Science and Exhibit, Reno, NV, USA, 2006

[5] P. Hartman, G. Minggione, "Prediction of ice accumulation and airfoil performance degradation: a Boeing – CIRA research collaboration", AHS 62th Annual Forum, Phoenix, Arizona, 2006

[6] H.M. Gurbacki, M.B. Bragg, "Unsteady aerodynamic measurements on an iced airfoil", 40th AIAA Aerospace Science and Exhibit, Reno, NV, USA, 2002

[7] Cambier L., Gazaix M. "*ElsA*: An efficient object-oriented solution to CFD complexity", 40th AIAA Aerospace Science and Exhibit, Reno, NV, USA, 2002

[8] Gerhold, T., Friedrich, O., Evans, J., Galle, M. "Calculation of Complex Three-Dimensional Configurations Employing the DLR-TAU-Code", AIAA-paper 97-0167, 1997

[9] O.J. Kwon, L.N. Sankar, "Numerical simulation of the flow about a swept wing with leading-edge ice accretion", Computer and fluids, Vol. 26, No. 2, pp. 183-192, 1997

[10] A.P. Broeren, M.B. Bragg, "Effect of residual and intercycle ice accretions on airfoil performance", Office of Aviation Research, Washington, D.C. 20591.